



**HAL**  
open science

## Searching for the nano effect in Cu-HCF (II) particles to improve Cs sorption efficiency: Highlighting the use of intrinsic magnetism

Micheàl Moloney, Clément Cabaud, Nicolas Massoni, Shelly Stafford, Yurii Gun'ko, Munuswamy Venkatesan, Agnès Grandjean

### ► To cite this version:

Micheàl Moloney, Clément Cabaud, Nicolas Massoni, Shelly Stafford, Yurii Gun'ko, et al.. Searching for the nano effect in Cu-HCF (II) particles to improve Cs sorption efficiency: Highlighting the use of intrinsic magnetism. *Colloids and Surfaces A: Physicochemical and Engineering Aspects*, 2019, 582, pp.123758. 10.1016/j.colsurfa.2019.123758 . cea-02389261

**HAL Id: cea-02389261**

**<https://cea.hal.science/cea-02389261>**

Submitted on 20 Jul 2022

**HAL** is a multi-disciplinary open access archive for the deposit and dissemination of scientific research documents, whether they are published or not. The documents may come from teaching and research institutions in France or abroad, or from public or private research centers.

L'archive ouverte pluridisciplinaire **HAL**, est destinée au dépôt et à la diffusion de documents scientifiques de niveau recherche, publiés ou non, émanant des établissements d'enseignement et de recherche français ou étrangers, des laboratoires publics ou privés.



Distributed under a Creative Commons Attribution - NonCommercial 4.0 International License

# Searching for the nano effect in Cu-HCF (II) particles to improve Cs sorption efficiency: Highlighting the use of intrinsic magnetism

Mícheál P. Moloney,<sup>a,b</sup> Clément Cabaud,<sup>a,e</sup> Nicolas Massoni,<sup>b</sup> Shelly Stafford,<sup>c</sup> Yurii K. Gun'ko,<sup>c</sup> Munuswamy Venkatesan,<sup>d</sup> Agnès Grandjean<sup>a</sup>

<sup>a</sup> CEA, DEN, Univ. Montpellier, DE2D, SEAD, Laboratory of Supercritical and Decontamination Processes, F-30207 Bagnols-sur-Cèze, France

<sup>b</sup> CEA, DEN, Univ. Montpellier, DE2D, SEVT, Research Laboratory for the development of conditioning matrices, F-30207 Bagnols-sur-Cèze, France

<sup>c</sup> School of Chemistry and Centre for Research on Adaptive Nanostructures and Nanodevices (CRANN) Institute, Trinity College Dublin, Dublin, Ireland

<sup>d</sup> School of Physics and Centre for Research on Adaptive Nanostructures and Nanodevices (CRANN) Institute, Trinity College Dublin, Dublin, Ireland

<sup>e</sup> MINES ParisTech, PLS Universtiy, Centre de Géosciences, F-77300 Fontainebleau

## Abstract

The silica templating of Cu-HexaCyanoFerrate (HCF) is a classical technique which is often used to control the size and monodispersity thereby increasing the exposed surface area, and therefore the Cs sorption efficiency of what are normally highly aggregated nanoparticle systems. However, here we show that long term magnetic agitation of unfunctionalised aggregated Cu-HCF nanoparticles leads to a uniform and stable colloidal dispersion. This, we believe, is due to the intrinsic magnetic nature of Cu-HCF as seen by low temperature SQUID measurements. In this work we see that the Cs kinetics of magnetically dispersed Cu-HCF show a remarkable increase in the rate Cs sorption due particle disaggregation. Finally, the Cs sorption kinetics of these magnetically disaggregated particles proved similar to a chemically similar monodisperse silica templated sample.

## Introduction

Transition metal hexacyanoferrates (HCF's) have attracted great interest over the last several decades from the nuclear sector. This interest is due to this materials ability to selectively extract trace amounts of radioactive Cs from waste water at varying pH's, and also in the presence of competitive ions at high concentration.[1-6] Prepared through a simple aqueous co-precipitation process, HCF's low toxicity combined with their aforementioned ability to quickly and selectively remove low concentrations of Cs from effluents which contain high concentrations of other  $M^{+1}$ , and  $M^{+2}$ , ions has made HCF's highly valuable materials. Here we look at copper (II) hexacyanoferrate (II) or simply Cu-HCF(II).

While Cu-HCF could be classified as a). an inorganic polymer, or b). a bimettic supramolecular complex, they are also in fact cube shaped nanoparticles with a generally reported size range of below 50 nm.[7, 8] However, problematically, a high degree of inter-particle aggregation exists in these materials.[6] Particle aggregation leads to a to a loss of exposed surface area and therefore can affect the Cs sorption kinetics. While nanoparticle aggregation is generally avoided through the use of surface bound stabilising molecules, this approach is (generally speaking) not used in the nuclear industry. The reasons for this are two-fold; firstly,the presence of such a molecular layer may inhibit Cs sorption, and secondly, the industry prefers that waste forms avoid the use of organic species due to the radiolysis effect. Instead HCF nanoscale is normally tuned by encasing, or growing, the HCF particles inside template materials. These templates can range from soft polymers to hard inorganic materials such as silica microspheres, or highly ordered silica monoliths.[6, 8-11] By employing template chemistry the particles are separated and dispersed throughout a porous template material thereby allowing for greater access to their surfaces. However, for financial reasons industrial setups are slow to adapt to new technologies and in fact aggregated HCFs are still used today to extract Cs from waste pools using physical aggregation to disperse the HCF in the effluent, and solid/liquid separation techniques to remove it once Cs has been extracted.[12] To our knowledge, there is a lack of an easy way to disaggregate HCF present as a suspension in aqueous solution.

In this paper, we propose to compare highly monodisperse Cu-HCF nanoparticles which were synthesised within the pores of a silica template to a "bulk" Cu-HCF suspensions, which has been disaggregated by the by the assistance of a magnetic field.[13] In the first part of this publication, we observe the spectroscopic properties (FT-IR, UV-Vis, XRD, and Elemental Analysis) of templated Cu-HCF nanoparticles and compared them to those of the highly aggregated Cu-HCF particle systems. The idea here is to determine if it is possible to elucidate any physical or chemical differences between the nano and bulk systems. If found, any electronic or structural differences, could then be discussed in relation to these materials ability to sorb Cs. In the second part, we propose a simple way to improve the extraction kinetics of bulk material without having to resort to template chemistry. The use of an external magnetic field to orientate or align magnetic particles is well recorded in the

literature but it normally involves superparamagnetic particles.[14-16] By simply applying a magnetic field to the aggregated particles it is possible to disaggregate them,[13] we then access their intrinsic nano-property of high surface area to mass ratio. This nano effect improves the rapid Cs sorption kinetics of these materials, [2, 6, 17] when compared with a true bulk material. In fact, recently a number of groups have begun to examine combining functionalisable magnetic nanoparticles and hexacyanoferrates to create two in one particles cable of magnetically [17] separating Cs from waste waters.[18-22] However, this functionalisation appears not necessary as Copper hexacyanoferrate (II) appears to be intrinsically magnetic (despite both metals being in the +2 oxidation state). We therefore report here for the first time that Cu-HCF can be affected by an external magnetic field without the need for further modification.

## Experimental

### Chemical products

All chemical products ( $\text{Cu}(\text{NO}_3)_2$ ,  $\text{K}_4[\text{Fe}(\text{CN})_6]$ ,  $\text{CsNO}_3$ , silica gel, 3-aminopropyl-triethoxysilane (APTES), solvent (acetone, ethanol) were purchased from Sigma-Aldrich. Potable mineral water that contains competitive cation was purchased from Evian<sup>®</sup>, and its mineral composition is given in supplementary information (SI).

### Analytical techniques

XRD data were recorded using a D8 Bruker Advance diffractometer (Cu  $\text{K}\alpha$  radiation). FT-IR and UV-Vis measurements were carried out using a Nicolet iS50 and Shimadzu UV-2600 respectively. TEM of the bulk particles was performed on a JEOL 2100 Lab TEM operating at 200 kV while the silica grain particles were examined using a Zeiss Leo EM910 operating at 120 kV. Chemical compositions were measured by inductively coupled mass spectrometry for Cu, Fe, K, Si after dissolution. Magnetisation measurements were carried using a SQUID magnetometer at both 300 K and 4 K, and thermal scans of the magnetisation in a 1 T field of the particles were examined were from 4 – 300 K.

### Stirrer/agitation

Several forms of mixing were used in the sorption study. In all cases bar one (mechanical stirring) the same vessel was used; 100 ml glass bottle. For mechanical stirring with a propeller stirrer a 250 ml beaker was used, as seen in Figure 3 of the SI.

The magnets used in this study were PTFE encased 12.4 g oval shaped magnetic stirrers purchased from VWR (VWRI422-0405). The dimensions of which were 300 mm x 16 mm. The stirring speed was set to 700 rpms. To mimic the mechanical effect of the magnetic stir bar without magnetic field, we use a plastic surrogate with a weigh and a size comparable to the one of the magnetic bar used. Rotary agitation was carried out using a Heidolph Reax 2,

purchased from Heidolph-Instruments. The instrument was set to speed 6. Mechanical stirring was carried out with a IKA labortechnik RW 20 DZM with power set to 65%.

### **Bulk Cu-HCF (II)**

Copper (II) Hexacyanoferrate (II) (here on referred to as Cu-HCF, or bulk Cu-HCF) was prepared by pouring 45 ml of an aqueous  $1 \times 10^{-1}$  M  $\text{Cu}(\text{NO}_3)_2 \cdot 3\text{H}_2\text{O}$  solution directly into 30 ml of a mixed aqueous solution of  $1 \times 10^{-1}$  M  $\text{K}_4[\text{Fe}(\text{CN})_6] \cdot 3\text{H}_2\text{O}$  (K-HCF) and  $1 \times 10^{-1}$  M  $\text{KNO}_3$ . Upon addition of the blue  $\text{Cu}(\text{NO}_3)_2 \cdot 3\text{H}_2\text{O}$  solution to the light yellow K-HCF/ $\text{KNO}_3$  solution a dark burgundy coloured precipitate was immediately formed. The contents of the reaction vessel were then allowed to mix for an hour by rotary mixing. The resulting solid was then collected by centrifugation and washed several times with Millipore water. As the washing steps accumulate the HCF-Cu becomes more and more stable in water and therefore equal volumes of acetone were needed as a non-solvent to help crash-out the particles. Once the washing steps are complete (4 washes) the Cu-HCF was dried under rotary evaporation at  $60^\circ\text{C}$ . The resulting dark solid was then examined using UV-Vis, FT-IR, XRD and TEM. Elemental analysis showed the structure formula to be  $\text{K}_{0.8}\text{Cu}_{1.58}\text{Fe}(\text{CN})_6 \cdot 4.8\text{H}_2\text{O}$

### **Cu-HCF (II) nano templated into Silica Grains**

Commercially available silica gel having a 15 nm mesoporosity was used as silica support. The gel was firstly functionalized with 3-aminopropyl-triethoxysilane (APTES). This was accomplished by dispersing the silica gel in an absolute ethanol solution and adding APTES. The resulting solution was stirred at  $60^\circ\text{C}$  for 24 hours. The  $-(\text{CH}_2)_3\text{-NH}_2$  functionalised silica gel was then washed several times with water and then acetone, in order to remove any unreacted APTES. The functionalised gel was then immersed in a  $1 \times 10^{-2}$  M copper nitrate solution and placed under rotary mixing for 2h. After washing with water, the now Cu functionalised silica gel was added to a  $1 \times 10^{-2}$  M  $\text{K}_4[\text{Fe}(\text{CN})_6] \cdot 3\text{H}_2\text{O}/\text{KNO}_3$  solution and allowed to stir for 2h. The as formed  $\text{Cu-HCF}@SiO_2$  gel was then washed with water. This two-step Cu-HCF impregnation process was repeated six times in total allowing for the growth of Cu-HCF on the silica surface(s). The resulting  $\text{Cu-HCF}@SiO_2$  grains were finally dried under air at  $40^\circ\text{C}$  for 48h. Elemental analysis performed as described in Michel et al.[23] showed the structure formula to be  $\text{K}_{1.36}\text{Cu}_{1.46}\text{Fe}(\text{CN})_6 \cdot 4.5\text{SiO}_2$ . This material is therefore 11.8% Cu-HCF and 88.2%  $\text{SiO}_2$  by mass.

### **Sorption experiments**

Simple Cs sorption experiments were carried in Evian<sup>®</sup> mineral water (composition in SI). This was done by first re-dispersing the Cu-HCF (or  $\text{Cu-HCF}@SiO_2$ ) in Evian<sup>®</sup> water. All batches contained 1g of Cu-HCF per 99 ml of mineral water and each batch was allowed to re-disperse overnight (see Table 1). Once particle dispersion was completed, the dispersions were then transferred to a magnetic stirring plate and a magnetic stirring bar was added and activated seconds before Cs solution addition. This Cs sorption reaction was initiated by addition of 1mL of a fixed concentration  $\text{CsNO}_3$ . This resulted in a solution  $70 \text{ mg}\cdot\text{L}^{-1}$  of  $\text{Cs}^+$

ions at the beginning of the sorption reaction for silica grains and batches 1 to 3 and 700 mg.L<sup>-1</sup> for batch 4. Aliquots of the resulting solution were taken at fixed intervals and filtered (the filters were 200 nm for the Cu-HCF and 450 nm for the Cu-HCF@SiO<sub>2</sub>) to remove the Cu-HCF (or Cu-HCF@SiO<sub>2</sub>) particles stopping the sorption process. The Cs concentration of each aliquot was then measured using a Perkin Elmer Analyst 400 atomic absorption spectrometer. This allowed us to monitor the Cs concentration against time.

The Cs sorption properties of hard templated Cu-HCF@SiO<sub>2</sub> particles were first compared to non-magnetically dispersed Cu-HCF particles. As described above the particles were dispersed in water overnight before Cs addition. Particle dispersion was performed using rotary agitation only (no magnet). This non-magnetically dispersed Cu-HCF sample is referred to as batch 1, where dispersion were done in presence of surrogate of stir bar (see below). The Cu-HCF@SiO<sub>2</sub> sample will henceforth be referred to as Gr or grain sample.[ Note : To aid contact time between the active sites in the nano Cu-HCF@SiO<sub>2</sub> particles and the Cs in solution the silica grain sample was firstly crushed down to  $\leq 20 \mu\text{m}$ ]. Once the particles were allowed to disperse for 19 hours the Cs sorption reaction was initiated as described above.

*Table 1 : Cs sorption data for bulk (B1-B4) and ground nano-templated silica grain (Gr) samples. Data has been normalised to account for actual Cu-HCF content as given by elemental analysis. Permanent Magnet and magnetic stirrer refers only to Cu-HCF dispersion*

	Cs init (mg.L <sup>-1</sup> )	Permanent magnet	Magnetic stirrer	Half Life (sec)	Capacity (mg/g) [%]**		
					At 20 seconds	At 1 min	Maximum
<b>Gr</b>	35			58	16[8]	112[52]	215*
<b>B1</b>	70			74	15[21]	33[45]	N/a
<b>B2</b>	70	X		6	61[84]	71[98]	N/a
<b>B3</b>	70	X	X	3	67[89]	74[98]	N/a
<b>B4</b>	700	X	X	14	143[54]	225[96]	266

\* Normalised with respect to % Cu-HCF in sample

\*\* the % of sorption capacity refers  $Q(t)/Q_{\text{max}}$  at equilibrium.

In order to study if a magnetic disaggregation effect as seen by Stuyven et al. was possible to induce, batches 2 and 3 were prepared.[13] Batches 2 and 3 were identical to batch 1 except for the following details (see Table 1). While batches 1 and 2 were in fact simultaneously dispersed using the same rotary mixer a magnetic stirrer (permanent magnet) was placed in batch 2 Batch 1 also contained a non-magnetic plastic object of similar size and shape to the stirring bar to mimic the magnetic stirrer (surrogate). Batch 3 was dispersed by conventional

magnetic stirring with no rotary mixing. After a 19 hours period of dispersion, the sorption reaction began as described above.

Finally the Cs sorption capacity of bulk Cu-HCF was determined by repeating the batch 3 experiment and increasing the initial Cs concentration by a factor of ten. This experiment is referred to as batch 4.

The sorption capacity was calculated by the classical formula

$$Q = ([Cs]_{init} - [Cs]_{final}) \frac{V}{m}$$

Where  $[Cs]_{init}$  and  $[Cs]_{final}$  are respectively the initial and final concentration of Cs in the solution ( $\text{mg}\cdot\text{L}^{-1}$ );  $V$  is the volume of solution used (L) and  $m$  the mass of solid used (g). In case of silica grain, this mass was taken equal to the mass of Cu-HCF inserted into the silica.

In each we report also the ratio (%) of Cs uptake by the solid at  $t$  (s or min): this ratio is equal to  $Q(t)/Q_{max}$  (%) where  $Q_{max}$  corresponds to the capacity at equilibrium for each batches.

## Results and Discussion

### Comparison between bulk and nano-templated Cu-HCF

#### XRD

The XRD patterns show that the Cu-HCF in both the unfunctionalised particles and the Cu-HCF@SiO<sub>2</sub> sample possessed a face centred cubic (FCC) structure with the space group Fm-3m. This corresponded to the PDF04-010-1963 card, i.e. K<sub>2</sub>CuFe(CN)<sub>6</sub> (see Figure 1). The amorphous state of silica is also confirmed. The backgrounds of the XRD patterns of Figure 1 were removed for clarity. The space group and lattice parameters are in good agreement with the literature.[24, 25] The lattice parameter of the bulk as-prepared sample was found to be  $10.0039 \pm 0.0040$  Å while the silica templated nano was quite similar at  $10.0007 \pm 0.0042$  Å. The smaller size of the templated HCF unit cell ( $-0.0032$  Å) is probably due to its relatively greater K<sup>+</sup> content, (see elemental analysis) as increased K<sup>+</sup> content has been reported to slightly reduce the lattice parameter.[25] However, despite this difference the near identical XRD patterns demonstrate that there is little structural difference between the materials formed by the two synthetic approaches (Figure 1).

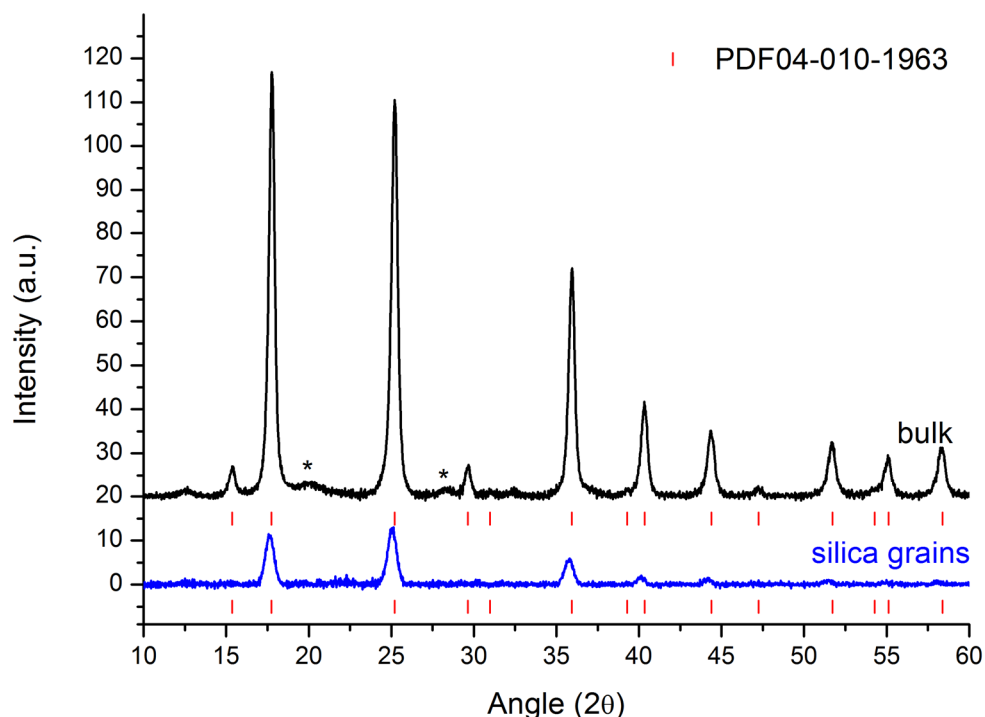


Figure 1: XRD of bulk (black) and silica grain (blue). The pattern backgrounds were removed to highlight the Cu-HCF reflections. Both samples possess a face centred cubic structure. The asterisks indicate the presence of impurities or secondary phases.

### FT-IR

FT-IR was carried out using a Nicolet iS50 infrared spectrometer. Looking firstly at the aggregated material, the  $\nu(\text{CN})$  stretch of the Cu-HCF is seen at  $2,089\text{ cm}^{-1}$ , (Figure 2-inset top centre). Cu-HCF (II) generally possesses a  $\nu(\text{CN})$  stretch at around  $2,095\text{ cm}^{-1}$ , while the  $\nu(\text{CN})$  stretch for Cu-HCF(III) (where the iron is in the  $\text{Fe}^{\text{III}}$  oxidation state) is typically located around  $2,177\text{ cm}^{-1}$ . [26, 27] Therefore, we can safely assume that Cu-HCF (II) is the dominant form here, (Figure 2). The  $\nu(\text{Fe-C})$  stretch is seen at  $594\text{ cm}^{-1}$ , (Figure 2-inset top right), this position again corresponds to the dominant presence of  $\text{Fe}^{\text{III}}$ . The  $\delta(\text{HOH})$  signal is seen at  $1,614\text{ cm}^{-1}$ , with a shoulder at  $1626\text{ cm}^{-1}$  indicating multiple water environments (Figure 2-inset bottom). The multiple structured  $\nu(\text{OH})$  signals which are seen above  $3,000\text{ cm}^{-1}$  confirm this assertion. This indicates the presence of several coordinated water sites. The boarder hump-like peak that they are buried in is indicative of zeolitic water, (Figure 2-inset top left). This is all in good agreement with the literature.

Moving to the templated (silica grain) sample, we see that the  $\nu(\text{CN})$  stretch has increased in frequency to  $2,103\text{ cm}^{-1}$ , (Figure 2-inset top centre). The  $\nu(\text{Fe-C})$  stretch has also increased in frequency to  $594\text{ cm}^{-1}$ , (Figure 2-inset top right). Despite these slight increases in frequency Cu-HCF (II) is also the dominant form in the templated sample. The  $\delta(\text{HOH})$  signal is seen at  $1,624\text{ cm}^{-1}$ , and is broad and tapering which suggests zeolitic water is more prevalence here, (Figure 2-inset bottom). This is confirmed by the  $\nu(\text{OH})$  signals which now consist of only a

single coordinated water peak at  $3,625\text{ cm}^{-1}$  and a broad zeolitic peak at  $3,412\text{ cm}^{-1}$ , (Figure 2-inset top left). As elemental analysis showed that the ratio of copper to iron was the same for the bulk and templated samples, that means that they have the same number of vacant  $\text{Fe}(\text{CN})_6^{4-}$  sites and therefore hydrated copper. This therefore indicates that the “other” coordinated water peaks in the bulk sample correspond to surface bound water; the surface coppers of the templated sample being bound to APTES’s  $-\text{NH}_2$  groups.

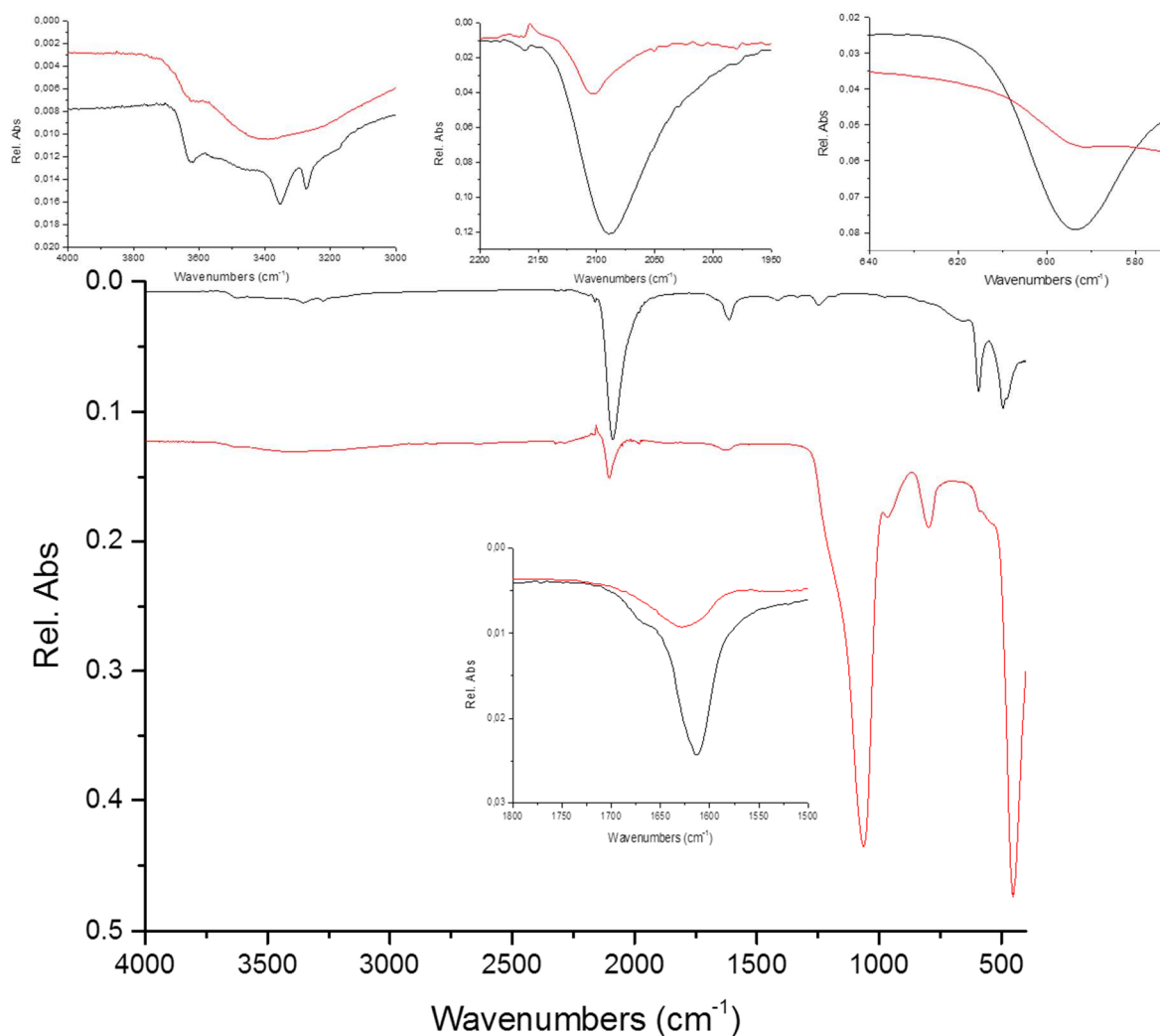


Figure 2 : FT-IR of as prepared templated Cu-HCF@silica-grains (red), and bulk Cu-HCF (black)). Close up of the  $\nu(\text{OH})$  (top left inset  $3,500\text{-}4,000\text{ cm}^{-1}$ ), cyano  $\nu(\text{CN})$  stretch (centre top inset -  $1,950\text{-}2,200\text{ cm}^{-1}$ ) and M-L stretches (top right inset -  $590\text{ cm}^{-1}$ ). The  $\delta(\text{HOH})$  close up is seen just below the main spectra.

Looking closer (Table 2) we see that the  $\nu(\text{CN})$  stretch of the nano-templated sample not only increases in the frequency by  $15\text{ cm}^{-1}$ , but that its full width half max (FWHM), decreases by  $25\text{ cm}^{-1}$ , when compared to the bulk. Taking the decrease in the FWHM first, the FWHM of the  $\nu(\text{CN})$  can be used to measure any change in the local chemical environment inside the

HCF cage. An increase in the chemical uniformity sees a decrease in FWHM, and vice versa. This effect was discussed in detail by Lejeune et al. where it was pointed out that the larger the guest ion the easier it is for it to “seen” by the greatest number of cyano bridging ligands.[28] The much narrower  $\nu(\text{CN})$  stretch of the templated sample is therefore probably due to its higher K content as seen in elemental analysis. It should be noted that the controlled growth of the particles on to the silica surface may also contribute to this sharper  $\nu(\text{CN})$  stretch. As for the  $\nu(\text{CN})$ 's relatively higher frequency, this suggests an enhanced interaction between the metals and CN ligands in the templated samples when compared to that of the bulk. Avila et al. saw similar high  $\nu(\text{CN})$  for Cu-HCF and pointed out that  $\text{Cu}^{2+}$  has the ability to fill its 3d shell by receiving electrons from the CN's 5 $\sigma$  orbital, thereby enhancing the bond strength and consequently causing a relative increase in the frequency of the  $\nu(\text{CN})$  stretch when compared with other HCF analogues.[29]

However, if this were the explanation here, why is this phenomenon not seen in the bulk samples? A likely explanation for the relatively higher frequency of the nano  $\nu(\text{CN})$  stretch is electron donation from the APTES amine groups to their adjacent coppers, strengthening the Cu-NC bonds which in turn effects the electronically sensitive cyano ligands. This would explain why the  $\nu(\text{Fe-C})$  stretches of both the templated and bulk samples occupy identical frequencies but the  $\nu(\text{CN})$ s do not.

*Table 2 :  $\nu(\text{CN})$  positons and full width half max (FWHM) values for aggregated (B) and grain (G) samples. K= as prepared. Cs = Caesium exchanged. All values are in  $\text{cm}^{-1}$ .*

	$\nu(\text{CN})$ B	$\nu(\text{CN})$ G	$\nu(\text{Fe-C})$ B	$\nu(\text{Fe-C})$ G
<b>Frequency (<math>\text{cm}^{-1}</math>)</b>	2089	2103	594	594
<b>FWHM (<math>\text{cm}^{-1}</math>)</b>	74	39	39	30.6

### Solid UV-Vis

The as-prepared bulk sample showed a broad peak at 476 nm and a narrower one at 319 nm, (Figure 3 and Table 3). A shoulder at 269 nm was also present. The signals at 319 nm and 269 nm can be assigned to  $\text{Fe}^{\text{III}}(\text{CN})_6$ , as they can also be seen in  $\text{K}_4\text{Fe}^{\text{III}}(\text{CN})_6$  starting material (SI).[30] The wider peak at 476 nm is assigned to Cu d-d transitions.[31, 32]

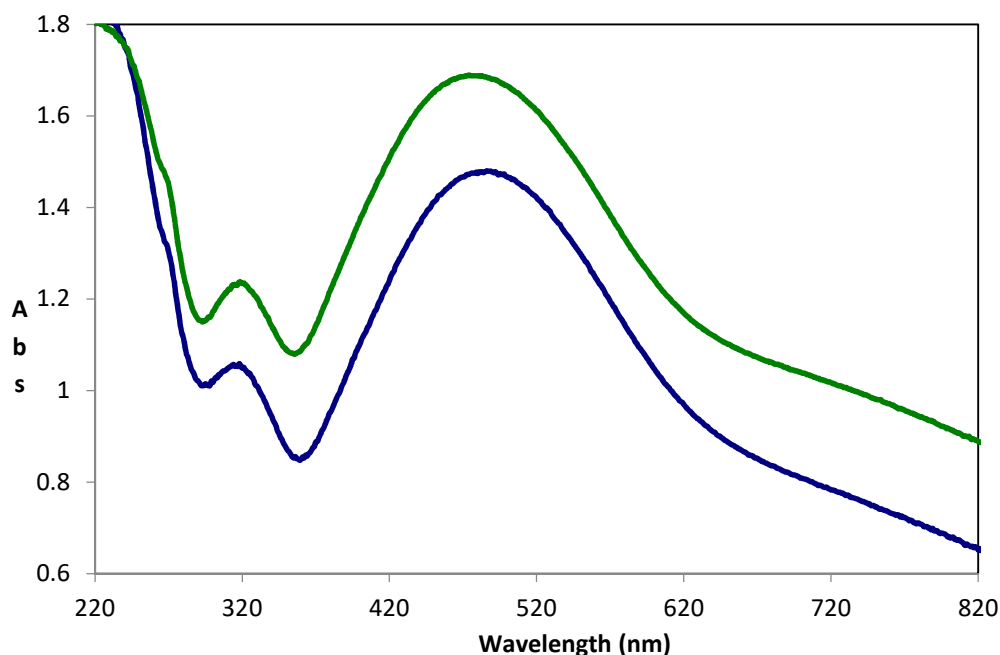


Figure 3 : Solid UV-Vis of as prepared bulk Cu-HCF (green) and Cu-HCF@silica-grain (blue).

The nano templated sample showed the Cu d-d peak at 483 nm and the ligand field (LF) bands of  $\text{Fe}^{\text{II}}(\text{CN})_6$  at 314 nm and 269 nm. The lower energy of the copper peak is probably due to the passivating effect of the APTES surface ligands while the higher energy of the Fe co-ordination sphere is probably due to the template effect as the  $\text{Fe}(\text{CN})_6$  units are forced to adjust to the coppers spacing in the silica surface. However, despite these variances in peak positions, again little difference is seen between the nano templated and as prepared bulk samples. This again indicates that the silica template has not altered the electronic properties of the Cu-HCF with respect to the aggregated sample.

Table 3 : UV-Vis data for bulk (b) and nano templated (g) samples. All values are in nm, (LF= Ligand Field)

Origin	State	Type	bulk (nm)	Templated (nm)
$\text{Fe}^{\text{II}}(\text{CN})_6$	${}^1\text{A}_{1g}{}^1\text{T}_{2g}$	LF	269	269
$\text{Fe}^{\text{II}}(\text{CN})_6$	${}^1\text{A}_{1g}{}^1\text{T}_{1g}$	LF	319	314
$\text{Cu}(\text{NC})_6$	$\text{E}_g\text{-T}_{2g}$	d-d	476	483

## TEM

TEM showed the bulk particles were heavily aggregated with a  $20 \text{ nm} \pm 5 \text{ nm}$ , (Figure 4). Templated particles inserted into silica grains were evaluated to be close to  $15 \pm 5 \text{ nm}$ , (Figure 4)

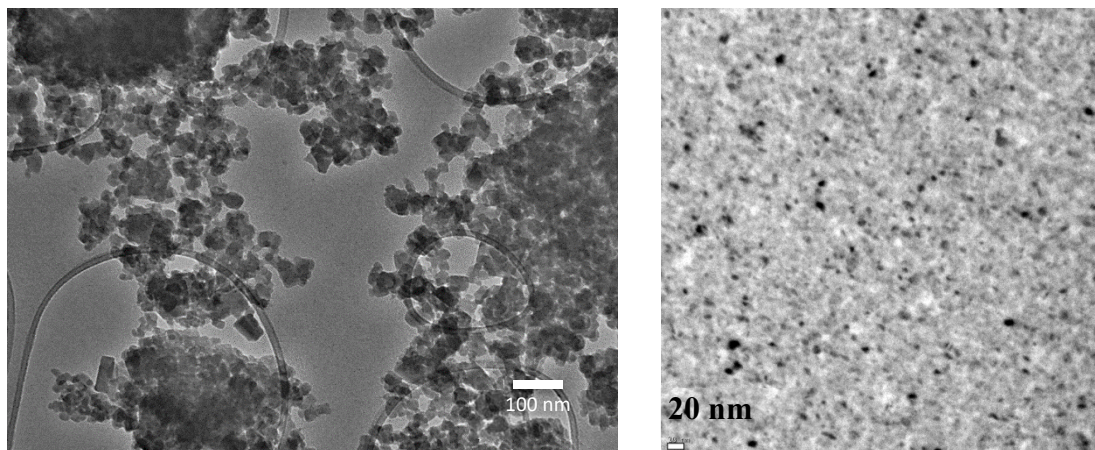


Figure 4: TEM of Cu-HCF Bulk particles (left) and templated (right). Average particles size is  $20 \text{ nm} \pm 5 \text{ nm}$  and  $15 \text{ nm} \pm 5 \text{ nm}$  respectively

## Cs Extraction Kinetics and Capacity

### Comparison bulk and nano-templated

As shown by spectroscopic analysis, it was realised that structurally there was very little difference between the templated and freely grown samples. In fact the only technique which showed a stark difference between the nano templated and bulk samples was TEM, (Figure 4), which showed, (as expected), that the unfunctionalised sample was heavily aggregated in contrast to the silica grains Cu-HCF@SiO<sub>2</sub> which contained individual pore based Cu-HCF particles.

The Cs extraction properties of the aggregated Cu-HCF (batch 1) were compared to those of the silica grain templated Cu-HCF@SiO<sub>2</sub> particles (batch Gr). This was done to determine if the increased monodispersity (and therefore increased surface availability) provided by nano-templating would increase the Cs sorption efficiency of Cu-HCF. When noting Cs sorption data one must remember that mg/g normally refers to mg of Cs sorbed per gram of Cu-HCF. Elemental analysis of the Cu-HCF@SiO<sub>2</sub> by ICP-MS (after dissolution of the sample) showed the chemical formula to be K<sub>1,36</sub>Cu<sub>1,46</sub>Fe(CN)<sub>6.45</sub>SiO<sub>2</sub> with the silica making up 88.2% by mass of the sample. Consequently, Cu-HCF makes up only around 11.8 % m/m of the Cu-HCF@SiO<sub>2</sub> sample, (Batch Gr). Therefore, unless otherwise stated all Cs sorption results for Cu-HCF@SiO<sub>2</sub> have been normalised to account of this.

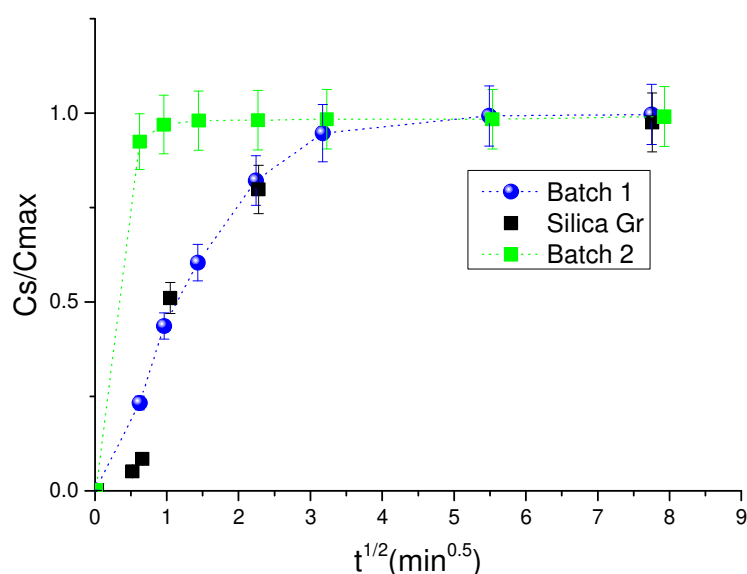


Figure 5: Cs sorption spectrum of batch 1 (no magnet, physical stirring) (blue circle), batch 2 (magnet, physical stirring) (green square) and Gr (silica grain) (black squares). Data is displayed as % Cs sorbed ( $C_s/C_{max}$  where  $C_s$  is concentration of Cs at time  $t$  and  $C_{max}$  is total Cs exchanged) against the square root of time.

Figure 5 shows the results of the kinetic experiment for the Cu-HCF (II) @ SiO<sub>2</sub> sample and batches 1 and 2. The Cs extraction kinetics of the silica templated particles are close to those of batch 1. The silica grain sample exchanges 52% of the total Cs added within 1 minute, while batch 1 exchange 45% at this time (see Table 1). Both sample (silica grain and aggregated) has reached near equilibrium at 10 minutes. However, Figure 5 also shows by applying a magnetic field to the particles (batch 2) and disaggregating them it is possible to enhance the Cs kinetics.

### Use of intrinsic magnetism to disaggregate Cu-HCF bulk suspension

It was observed over the course of this study that the batch 1 rotary dispersed Cu-HCF particles separate and disperse far more uniformly if a magnetic stirrer is included. By casual observation it appeared that after 3 hours a black homogenous dispersion was acquired. In fact, once rotary aggregation was halted after 19 hours the magnet containing (batch 2) sample did not immediately flocculate, unlike batch 1, (Figure 6). After this was observed attempts were made to disperse Cu-HCF particles, again using a Heidolph Reax 2, but this time including an object of similar composition, shape and size to a magnetic stirrer to determine if it was the magnetic nature of the stirrer, or simply the presence of a “grinding assistant”, which aided dispersion (Figure 6). However, the presence of a non-magnetic surrogate had no effect. Mechanical stirring was also tried but again did not produce a homogenous dispersion (SI). The only other technique which yielded similar results was when the particles were dispersed by classic magnetic stirring (batch 3). The Cs extracting abilities of magnetically dispersed Cu-HCF (batches 2 and 3) were then examined and compared non-magnetically dispersed (batch 1).



*Figure 6 : Photograph of as-prepared Cu-HCF nanoparticles. Particles were prepared, dried, weighed, and then redispersed in water. Each bottle contains 1 g of Cu-HCF in 100 ml of commercially available mineral water, (composition in SI). The image was taken immediately after both samples were removed from the same rotary agitator. They had previously spent 4 days undergoing rotary mixing. . This far longer mixing time was used to remove any ambiguity. The bottle on the right had a magnetic stirring bar placed in it before rotary mixing began (batch 2). These particles were fully dispersed after 3 hours. The one on the left (batch 1) acted as a control contained a non-magnetic plastic object of similar size and shape to the stirring bar.*

Magnetic dispersion is characterised as either active, (under magnetic stirring (batch 3)), or passive (physically agitated in the presence of a permanent magnet (batch 2)). For the non-magnetically dispersed sample a plastic Eppendorf (filled with water) was added to mimic the stirring bar's size and shape (batch 1).

Figure 7 shows the resulting sorption trace in a form of the diffusing model first proposed by Morris and Weber.[33] In it milligrams of Cs sorbed per gram of Cu-HCF are plotted against the square root of time (minutes). This model allows for the determination of the diffusive limiting step of a sorption by a solid. That is the diffusion of ions in solution, followed by their diffusion in the transition layer between the liquid and solid (called boundary layer), and then through the solid (intra-particle diffusion). The initial measurement was taken 20 seconds after contact with the dispersed Cu-HCF. The final measurement was taken after an hour, by which time all three batches (1-3) had almost completely sorbed the total added Cs. As seen in Table 1, batch 1 (no magnet and physical stirring) showed 45 % Cs sorption after one minute (close to sorption half-life). However, while initial sorption was quite fast, it began to rapidly slow with 18 % of the total sorbed Cs still remaining after 5 minutes (Figure 7). Near total sorption was completed between 10 and 30 minutes. These results plus the shape of the sorption curve would indicate a 2 or even 3 step process, as describe elsewhere.[34] We believe that step 1 is probably the rapid removal of Cs from the solution by exchanging it with the K ions present on, and close to, the aggregated HCF's surface. This initial exchange is accomplished in the first minute. This is then followed by a slower ion diffusion process as the sorbed Cs is exchanged with K held deeper in the HCF cage structure (intraparticle diffusion). Once this internal exchange (with K now once again close to the

surface) is complete the removal of Cs from solution begins again. This process is continued until all Cs has been removed from the surrounding solution.

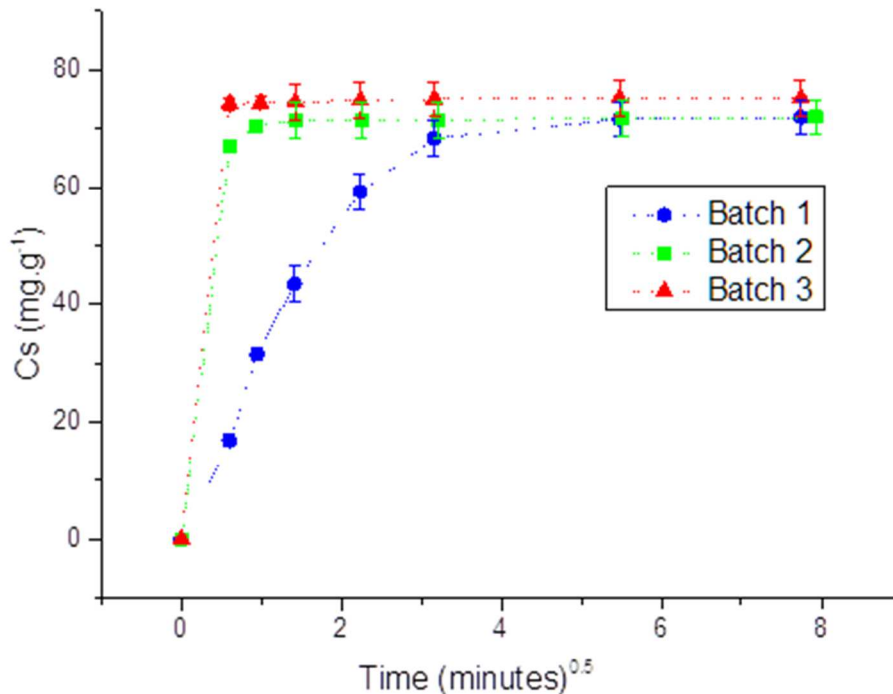


Figure 7 : Cs sorption spectrum of aggregated batch 1 (no magnet, physical stirring-red circles), batch 2 (with magnet but physical agitated-black squares) and batch 3 (with magnet and magnetically stirred- blue triangles). Data is displayed as mg Cs sorbed per gram of Cu-HCF against the square root of time.

The addition of a magnet has a drastic effect on the sorption kinetics. Batch 2 (again dispersed by rotary agitation, but now in the presence of a permanent magnet) displayed an enhanced Cs sorption kinetic. The sorption half-life was calculated at 6 seconds, while 84 % of the total Cs has been sorbed within the first 20 seconds and 98 % within the first minute. Batch 2 seems also to exhibit a 2 step process, with over double the time required to sorb the remaining 50% of the solutions Cs, however, as this batches sorption half-life is over an order of magnitude greater than batch 1, (6 vs 74 seconds) almost total sorption is complete within two minutes. Finally, the dispersion which had been magnetically stirred overnight (batch 3) had sorbed 89 % of the total Cs<sup>+</sup> after 20 seconds, this increased to 98% by the end of the first minute. Its half-life was recorded as 3 seconds. This is twice as fast as batch 2.

After 30 minutes all three batches contained around 0.5 ppm of Cs indicating that the equilibrium point is not affected by the dispersion method. As is clear the slow Cs/K diffusion step is present in batch 2. However, thanks to its uniform dispersion, and therefore better access to each particles individual surface, ultra-fast sorption of 99 % of the Cs content is achieved within 60 seconds after contact with the sorbent. While it would be easy to assume

the improved dispersion of batches 2 and 3 are simply a result of the difference between magnetic stirring and rotary mixing, the lack of a magnetic stirring plate in batch 2 demonstrates that it is in fact the presence of an external permanent magnetic field within the container aided by rotary agitation that allows the Cu-HCF particles to disaggregate. Once disaggregated the Cu-HCF particles arrange themselves more homogeneously (throughout the magnetic field) allowing the Cs<sup>+</sup> ions a more unobstructed access to their surfaces. The presence of an alternating field in batch 3 further improves this effect.

#### Capacity Kinetics

Once normalised for % mass of Cu-HCF, the Cs capacity of the Cu-HCF@SiO<sub>2</sub> was found to be around 215 mg/g. Therefore to determine capacity of the bulk sample the batch 3 experiment was repeated using a 700 ppm Cs solution (from now on referred to as batch 4). From this experiment the capacity of the bulk sample was determined to be 266 mg/g, (after one day). This high concentration experiment also allowed us to compare the Cs sorption kinetics at capacity of disaggregated bulk against the silica templated particles.

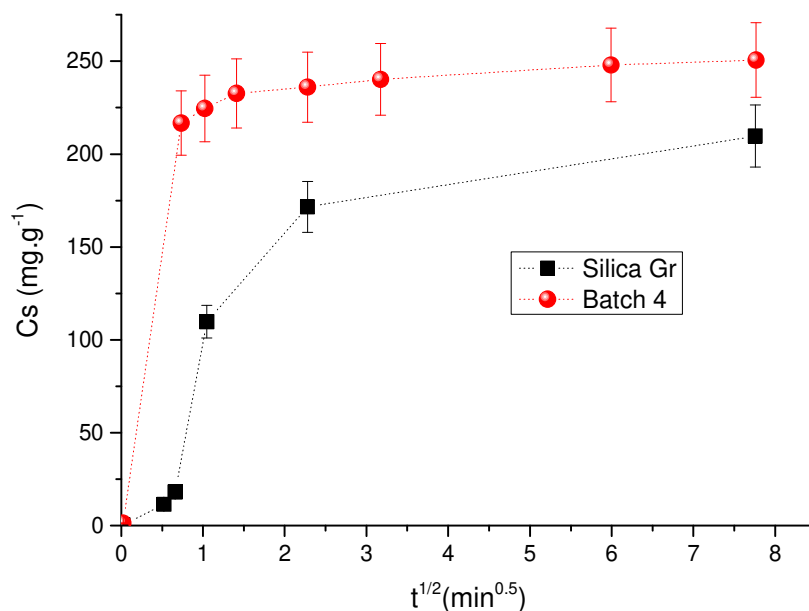


Figure 8 : Cs capacity sorption spectrum of Cu-HCF batch 4 (red circles). The black squares show Cs sorption onto crushed Cu-HCF @ silica grains. Data is displayed as  $C_s/C_{max}$  of Cs against the square root of time. Silica grain sorption data has been normalised according to amount of HCF particles per gram of crushed grain (11%).

Batch 4 showed a sorption half-life of 14 seconds, and within the first minute of contact with the Cs solution it had sorbed 96% of the total sorbed Cs, (Figure 8 and Table 1). [This is in agreement with batch 3 and shows the reproducibility of these experiments in both high and low concentration Cs solutions]. Compared to Cu-HCF@SiO<sub>2</sub> batch (Gr) which showed a Cs sorption half-life of 58 seconds, and 52 % Cs sorbed in one minute, we see that batch 4 is far more efficient. Cs measurements at equilibrium showed that batch 4 had sorbed 266 mg of Cs per gram of Cu-HCF. For the silica samples, once normalised the grains showed a Cs sorption capacity of 215 mg/g. These results were unusual as the templated sample should have shown a much quicker sorption kinetic than the bulk sample, unless of course the bulk sample was as disperse as the templated one. The capacity of batch 4 is also higher than the Cu-HCF@SiO<sub>2</sub> Gr batch. This difference however falls within human/experimental error. This result clearly shows the benefit of the dispersion of bulk samples assisted by a magnetic field.

### SQUID

Magnetisation measurements were carried out on the bulk Cu-HCF (II) particles (Figure 9) and confirmed that the particles are paramagnetic. Powder samples (bulk Cu-HCF samples) were mounted in gel caps, which have a temperature – independent diamagnetic susceptibility of  $-5.9 \cdot 10^{-9} \text{ m}^3 \text{ kg}^{-1}$ . The magnetisation curve at 300 K and 4 K is shown in Figure 9, after correction for the diamagnetism of the sample holder. The curve is linear and paramagnetic at 300 K, with no trace of ferromagnetic behaviour. The paramagnetic contribution at 4 K can be well fitted by Brillouin function [Fe<sup>(III)</sup> and J = 4]:

$$M(x) = NJ\mu_B g_J \left[ \frac{2J+1}{2J} \coth\left(\frac{2J+1}{2J}x\right) - \frac{1}{2J} \coth\left(\frac{1}{2J}x\right) \right] \quad (1)$$

where  $x = g_J J \mu_B H_e / k_B T$  is the ratio of the Zeeman energy of the magnetic moment in the effective field  $H_e$  to the thermal energy, the effective field  $H_e = H + H_m$ , where the  $H_m$  is the molecular field proportional to magnetic moment  $M$ ,  $g_J$  is the g-factor,  $J$  the angular momentum number,  $N$  the number of spins,  $k_B$  the Boltzmann constant. The paramagnetic moment per iron atom obtained from fitting the Brillouin function to the magnetisation at 5K is  $4.8 \mu_B$ .

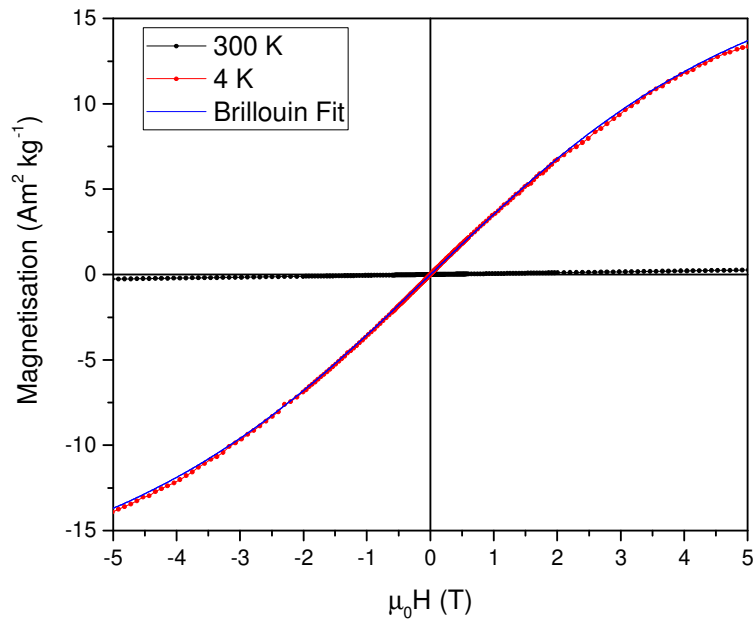


Figure 9: Magnetisation data of Cu-HCF aggregated particles at 300 K and 4 K

Figure 10 shows the magnetisation data of aggregated particles, as a function of temperature in an applied magnetic field of 100 mT. Furthermore the plot of the inverse susceptibility (Figure 10 b), there is no clear magnetic transition and the samples exhibit paramagnetic behaviour. The susceptibility is fitted to the equation  $\chi(T) = \chi_0 + \chi_{CW}(T)$  between 4 K and 100 K. Here  $\chi_0$  is the temperature independent term and  $\chi_{CW}(T) = C/(T - \Theta_{CW})$  is the Curie-Weiss term with Curie constant  $C = N_A p_{eff}^2 \mu_B^2 / (3k_B)$  and Curie-Weiss temperature  $\Theta_{CW}$  ( $N_A$  is Avogadro number,  $p_{eff}$  is the effective Bohr magneton number,  $\mu_B$  is the Bohr magneton, and  $k_B$  is the Boltzmann constant). The effective magnetic moment  $p_{eff}$ , obtained from the Curie law to the magnetisation versus temperature data, is  $4.7 \mu_B$ . These values agree but are slightly lower than what would be expected if all the iron in the sample were present as high spin  $Fe^{2+}$  ions (typically  $5.4 \mu_B$ ). Although Mössbauer spectroscopy would be needed to elucidate the exact spin state of the Fe it was not carried out as SQUID was determined to be sufficient to show that Cu-HCF particles are indeed magnetic. Finally, it should be noted that there is a large paramagnetic contribution arising from Cu(II) ions, as illustrated by the non-saturated paramagnetic behaviour in magnetization curves, both in field and temperature dependent magnetization curves.[35, 36]

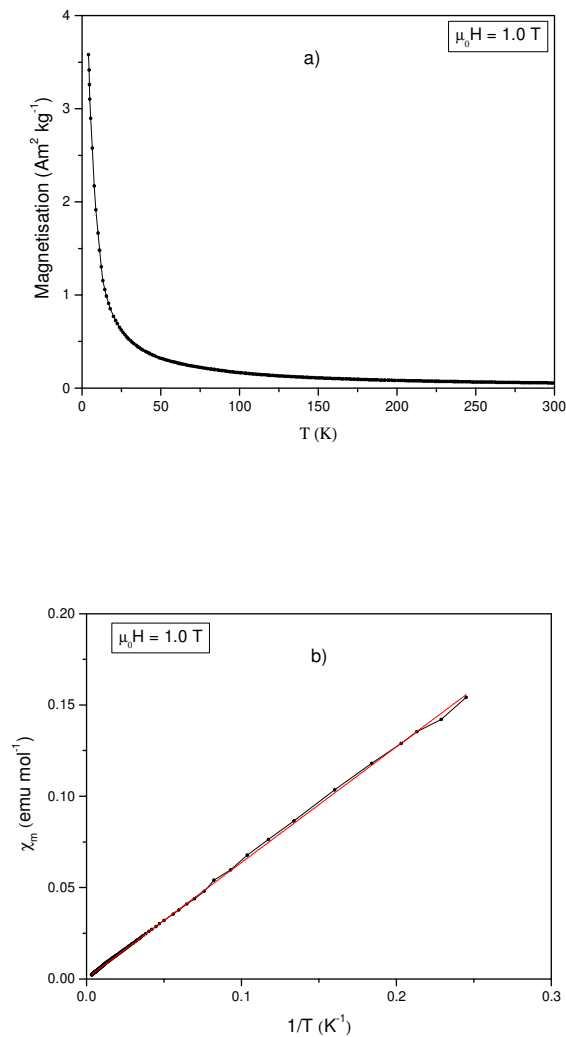


Figure 10 : Above, temperature dependence of magnetisation of aggregated particles as a function of  $T$ . Below, temperature dependence of magnetic susceptibility ( $\chi_m$ ) of aggregated particles as a function of  $1/T$ .

As Corr et al. have previously shown it is possible to disaggregate magnetic particles and align individual super paramagnetic particles in an applied field.[15] We believe that this goes some way to explaining how the presence of paramagnetism aides in the disaggregation of the Cu-HCF particles. However going further Stuyven et al pointed out that the stability of a suspension of charged particles can be seen as being in dynamic equilibrium between van der Waals (attractive) forces and electrostatic repulsion.[13] By placing the particles under rotary mixing the number of aggregate collisions, as well as the hydrodynamic sheer stress, will be increased causing the aggregates to disassemble. Eventually reaching equilibrium the frequency of aggregate growth and break up will define the mean aggregate size. The addition of an external magnetic field will complicate this. The addition of accompanying Lorentz forces will affect the van der Waals/electrostatic balance

as the Lorentz forces act on opposite directions of opposite sides of rotating charged particles separating them. This will also enhance the effect of sheer stress as they move from the inside to the outside of the moving container (and back again). This due to the difference in local velocity gradients along the container walls.

## Conclusion

Cu-HCF nanoparticles were prepared by two routes, the classic co-precipitation method, and grown step by step inside silica grains. XRD, FT-IR and UV-Vis measurements demonstrated that the aggregated Cu-HCF and the more monodisperse Cu-HCF@SiO<sub>2</sub> particles are chemically near identical. Comparison of the Cs sorption kinetics show that by using a magnetic field to aid with the dispersal of the aggregated particles the time taken to sorb 50% of the total Cs was decreased from over a minute to 6 seconds, with total sorption time being almost complete after 60 seconds instead of 10 minutes. By comparing the aggregated HCF and ground silica sample we see that the silica templated particles are the more efficient of the two, sorbing 53% of the total Cs after 1 minute compared to the aggregated samples 44%. However, once the aggregated particles are magnetically dispersed the sample efficiency increases to 96-98% of total Cs sorbed after 1 minute. This implies we have dispersed the Cu-HCF particles within a magnetic template equaling the monodispersity of the silica template.

## Author Information

### Corresponding Author

Agnès GRANDJEAN, CEA, DEN, Univ. Montpellier, DE2D, SEAD, Laboratory of Supercritical and Decontamination Processes, F-30207 Bagnols-sur-Cèze, France.

E-mail: [agnes.grandjean@cea.fr](mailto:agnes.grandjean@cea.fr)

### Author Contributions

The manuscript was written through contributions of all authors. All authors have given approval to the final version of the manuscript.

### Funding Sources

Research was conducted in part by the Center for Hierarchical Waste Form Materials (CHWM), an Energy Frontier Research Center (EFRC) supported by the U.S. Department of Energy, Office of Basic Energy Sciences, Division of Materials Sciences and Engineering under Award DE-SC0016574. We also thank the EDDEM-CEA project for funding this work.

## Acknowledgements

Elemental Analysis was carried out by the Laboratoire de metallographie et d'analyse chimique, DEN/MAR/SA2I/DIR, CEA Marcoule, France.

## Data Availability

The raw/processed data required to reproduce these findings cannot be shared at this time due to technical or time limitations

## References

- [1] H. Draouil, L. Alvarez, J. Causse, V. Flaud, M.A. Zaibi, J.L. Bantignies, M. Oueslati, J. Cambedouzou, Copper hexacyanoferrate functionalized single-walled carbon nanotubes for selective cesium extraction, *New Journal of Chemistry*, 41 (2017) 7705-7713.
- [2] A. Grandjean, C. Delchet, J. Causse, Y. Barré, Y. Guari, J. Larionova, Effect of the chemical nature of different transition metal ferrocyanides to entrap Cs, *Journal of Radioanalytical and Nuclear Chemistry*, 307 (2016) 427-436.
- [3] D.H. Ding, Z.Y. Zhang, Z.F. Lei, Y.N. Yang, T.M. Cai, Remediation of radiocesium-contaminated liquid waste, soil, and ash: a mini review since the Fukushima Daiichi Nuclear Power Plant accident, *Environmental Science and Pollution Research*, 23 (2016) 2249-2263.
- [4] K.-M. Lee, T. Kawamoto, K. Minami, A. Takahashi, D. Parajuli, G. Kido, K. Yoshino, H. Tanaka, Improved adsorption properties of granulated copper hexacyanoferrate with multi-scale porous networks, *RSC Adv.*, 6 (2016) 16234-16238.
- [5] I. Bokor, S. Sdraulig, P. Jenkinson, J. Madamperuma, P. Martin, Development and validation of an automated unit for the extraction of radiocaesium from seawater, *Journal of Environmental Radioactivity*, 151 (2016) 530-536.

- [6] J. Causse, A. Tokarev, J. Ravaux, M. Moloney, Y. Barre, A. Grandjean, Facile one-pot synthesis of copper hexacyanoferrate nanoparticle functionalised silica monoliths for the selective entrapment of Cs-137, *Journal of Materials Chemistry A*, 2 (2014) 9461-9464.
- [7] R.N. Soek, A. Schmidt, H. Winnischofer, M. Vidotti, Anisotropic behavior of layer-by-layer films using highly disordered copper hexacyanoferrate(II) nanoparticles, *Applied Surface Science*, 378 (2016) 253-258.
- [8] L. Catala, T. Mallah, Nanoparticles of Prussian blue analogs and related coordination polymers: From information storage to biomedical applications, *Coordination Chemistry Reviews*, 346 (2017) 32-61.
- [9] C. Loos-Neskovic, C. Vidal-Madjar, B. Jimenez, A. Pantazaki, V. Federici, A. Tamburini, M. Fedoroff, E. Persidou, A copper hexacyanoferrate/polymer/silica composite as selective sorbent for the decontamination of radioactive caesium, *Radiochim. Acta*, 85 (1999) 143-148.
- [10] A. Sommer-Marquez, C. Mansas, N. Talha, C. Rey, J. Causse, Reinforced silica monoliths functionalised with metal hexacyanoferrates for cesium decontamination: a combination of a one-pot procedure and skeleton calcination, *RSC Adv.*, 6 (2016) 73475-73484.
- [11] R. Turgis, G. Arrachart, C. Delchet, C. Rey, Y. Barre, S. Pellet-Rostaing, Y. Guari, J. Larionova, A. Grandjean, An Original "Click and Bind" Approach for Immobilizing Copper Hexacyanoferrate Nanoparticles on Mesoporous Silica, *Chem. Mat.*, 25 (2013) 4447-4453.
- [12] J. Flouret, Y. Barre, H. Muhr, E. Plasari, Design of an intensified coprecipitation reactor for the treatment of liquid radioactive wastes, *Chemical Engineering Science*, 77 (2012) 176-183.
- [13] B. Stuyven, Q.H. Chen, W. Van de Moortel, H. Lipkens, B. Caerts, A. Aerts, L. Giebelier, B. Van Eerdenbrugh, P. Augustijns, G. Van den Mooter, J. Van Humbeeck, J. Vanackem, V.V. Moshchalkov, J. Vermant, J.A. Martens, Magnetic field assisted nanoparticle dispersion, *Chemical Communications*, (2009) 47-49.
- [14] M. Tanase, L.A. Bauer, A. Hultgren, D.M. Silevitch, L. Sun, D.H. Reich, P.C. Searson, G.J. Meyer, Magnetic Alignment of Fluorescent Nanowires, *Nano Letters*, 1 (2001) 155-158.
- [15] S.A. Corr, S.J. Byrne, R. Tekoriute, C.J. Meledandri, D.F. Brougham, M. Lynch, C. Kerskens, L. O'Dwyer, Y.K. Gun'ko, Linear Assemblies of Magnetic Nanoparticles as MRI Contrast Agents, *Journal of the American Chemical Society*, 130 (2008) 4214-4215.
- [16] Q. Dai, A. Nelson, Magnetically-responsive self assembled composites, *Chemical Society Reviews*, 39 (2010) 4057-4066.
- [17] S. Ayrault, B. Jimenez, E. Garnier, M. Fedoroff, D.J. Jones, C. Loos-Neskovic, Sorption Mechanisms of Cesium on  $\text{CuII2FeII(CN)6}$  and  $\text{CuII3[FeIII(CN)6]2}$  Hexacyanoferrates and Their Relation to the Crystalline Structure, *Journal of Solid State Chemistry*, 141 (1998) 475-485.
- [18] H.G. Mobtaker, S.M. Pakzad, T. Yousefi, Magnetic CuHCNPAN nano composite as an efficient adsorbent for strontium uptake, *Journal of Nuclear Materials*, 504 (2018) 55-60.
- [19] H.M. Yang, K.S. Hwang, C.W. Park, K.W. Lee, Sodium-copper hexacyanoferrate-functionalized magnetic nanoclusters for the highly efficient magnetic removal of radioactive caesium from seawater, *Water Research*, 125 (2017) 81-90.
- [20] K.S. Hwang, C.W. Park, K.W. Lee, S.J. Park, H.M. Yang, Highly efficient removal of radioactive cesium by sodium-copper hexacyanoferrate-modified magnetic nanoparticles, *Colloids and Surfaces a-Physicochemical and Engineering Aspects*, 516 (2017) 375-382.
- [21] H.G. Mobtaker, T. Yousefi, S.M. Pakzad, Cesium removal from nuclear waste using a magnetical CuHCNPAN nano composite, *Journal of Nuclear Materials*, 482 (2016) 306-312.
- [22] H. Zhang, X. Zhao, J. Wei, F. Li, Sorption behavior of cesium from aqueous solution on magnetic hexacyanoferrate materials, *Nuclear Engineering and Design*, 275 (2014) 322-328.
- [23] C. Michel, Y. Barré, L. De Windt, C. de Dieuleveult, E. Brackx, A. Grandjean, Ion exchange and structural properties of a new cyanoferrate mesoporous silica material for Cs removal from natural saline waters, *Journal of Environmental Chemical Engineering*, 5 (2017) 810-817.
- [24] D.O. Ojwang, J. Grins, D. Wardecki, M. Valvo, V. Renman, L. Häggström, T. Ericsson, T. Gustafsson, A. Mahmoud, R.P. Hermann, G. Svensson, Structure Characterization and Properties of K-Containing Copper Hexacyanoferrate, *Inorganic Chemistry*, 55 (2016) 5924-5934.

- [25] J.-Y. Liao, Q. Hu, B.-K. Zou, J.-X. Xiang, C.-H. Chen, The role of potassium ions in iron hexacyanoferrate as a cathode material for hybrid ion batteries, *Electrochimica Acta*, 220 (2016) 114-121.
- [26] C.W. Ng, J. Ding, Y. Shi, L.M. Gan, Structure and magnetic properties of copper(II) hexacyanoferrate(III) compound, *Journal of Physics and Chemistry of Solids*, 62 (2001) 767-775.
- [27] S.N. Ghosh, Infrared spectra of the Prussian blue analogs, *Journal of Inorganic and Nuclear Chemistry*, 36 (1974) 2465-2466.
- [28] J. Lejeune, J.-B. Brubach, P. Roy, A. Bleuzen, Application of the infrared spectroscopy to the structural study of Prussian blue analogues, *Comptes Rendus Chimie*, 17 (2014) 534-540.
- [29] M. Avila, L. Reguera, J. Rodríguez-Hernández, J. Balmaseda, E. Reguera, Porous framework of  $T_2[Fe(CN)_6] \cdot xH_2O$  with  $T=Co, Ni, Cu, Zn$ , and  $H_2$  storage, *Journal of Solid State Chemistry*, 181 (2008) 2899-2907.
- [30] H.B. Gray, N.A. Beach, The Electronic Structures of Octahedral Metal Complexes. I. Metal Hexacarbonyls and Hexacyanides, *Journal of the American Chemical Society*, 85 (1963) 2922-2927.
- [31] R.S. Babu, P. Prabhu, S.S. Narayanan, Facile immobilization of potassium-copper hexacyanoferrate nanoparticles using a room-temperature ionic liquid as an ionic binder and its application towards BHA determination, *Journal of Solid State Electrochemistry*, 20 (2016) 1575-1583.
- [32] A. Tokarev, P. Agulhon, J. Long, F. Quignard, M. Robitzer, R.A.S. Ferreira, L.D. Carlos, J. Larionova, C. Guerin, Y. Guari, Synthesis and study of Prussian blue type nanoparticles in an alginate matrix, *Journal of Materials Chemistry*, 22 (2012) 20232-20242.
- [33] W.J. Weber, J.C. Morris, Kinetics of adsorption on carbon from solution, *Journal of the Sanitary Engineering Division*, 89 (1963) 31-59.
- [34] H. Zhu, J. Yuan, X. Tan, W. Zhang, M. Fang, X. Wang, Efficient removal of  $Pb^{2+}$  by Tb-MOFs: identifying the adsorption mechanism through experimental and theoretical investigations, *Environmental Science: Nano*, 6 (2019) 261-272.
- [35] P. Cheng, D. Liao, S. Yan, Z. Jiang, G. Wang, Paramagnetic and diamagnetic binuclear copper(II) complexes with different bidentate exogenous bridges: synthesis, spectroscopy and magnetic properties, *Transition Metal Chemistry*, 21 (1996) 515-518.
- [36] M. Okubo, D. Asakura, Y. Mizuno, T. Kudo, H. Zhou, A. Okazawa, N. Kojima, K. Ikeda, T. Mizokawa, I. Honma, Ion-Induced Transformation of Magnetism in a Bimetallic CuFe Prussian Blue Analogue, *Angewandte Chemie International Edition*, 50 (2011) 6269-6273.

